## Tailoring Fusion-Based Error Correction for High Thresholds to Biased Fusion Failures

Kaavya Sahay<sup>®</sup>, Jahan Claes<sup>®</sup>, and Shruti Puri

Department of Applied Physics, Yale University, New Haven, Connecticut 06511, USA

and Yale Quantum Institute, Yale University, New Haven, Connecticut 06511, USA

(Received 2 February 2023; accepted 26 June 2023; published 21 September 2023)

We introduce fault-tolerant (FT) architectures for error correction with the XZZX cluster state based on performing measurements of two-qubit Pauli operators  $Z \otimes Z$  and  $X \otimes X$ , or *fusions*, on a collection of few-body entangled resource states. Our construction is tailored to effectively correct noise that predominantly causes faulty  $X \otimes X$  measurements during fusions. This feature offers a practical advantage in linear optical quantum computing with dual-rail photonic qubits, where failed fusions only erase  $X \otimes X$  measurement outcomes. By applying our construction to this platform, we find a record-high threshold to fusion failures exceeding 25% in the experimentally relevant regime of nonzero loss rate per photon, considerably simplifying hardware requirements.

DOI: 10.1103/PhysRevLett.131.120604

Introduction.—Fault-tolerant (FT) error correction enables arbitrary suppression of errors when the error rate is below a constant threshold, making scalable quantum computation possible. Considering the available underlying physical operations facilitates efficient FT architecture design. If the entangling operations are inherently probabilistic or if the noise in these operations destroys qubits, then measurement-based error correction (MBEC) is natural [1–3].

MBEC is implemented using a *cluster state* [4–8], a many-body entangled state that may be obtained by *foliating* a stabilizer code [9–12]. Outcomes of single-qubit measurements performed on the cluster state are used to reconstruct the underlying stabilizers and correct errors [9,13]. The well-known Raussendorf-Harrington-Goyal (RHG) cluster state [9,13,14] is a foliation of the standard surface code [15]. Recently, the *XZZX* cluster state was introduced [16], which is a foliation of the *XZZX* surface code [17,18].

The cluster state may be generated using a set of commuting two-qubit entangling gates. Alternatively, one can start with a collection of few-body entangled states and stitch them into a cluster state using Bell measurements, or measurements of two-qubit operators  $X \otimes X$  and  $Z \otimes Z$ , also called fusions; these may be implemented destructively [19]. This approach has been termed fusion-based error correction (FBEC) [3] and is a natural choice for platforms where high-fidelity fusions are native, like dual-rail photonic qubits [19], continuous variable qubits [20,21], and Majorana qubits [22]. The FBEC framework has been studied for error correction with the RHG cluster state [3,23] and, recently, with the foliated Floquet color code [24].

In this Letter, we introduce two fusion-based constructions for error correction with the XZZX cluster state, one based on fusing together four-qubit entangled resource states and the other based on fusing six-qubit resource states. Both constructions offer higher thresholds when noise in the fusion circuit is biased so that  $Z \otimes Z$  measurements are more reliable than  $X \otimes X$ . This is because faulty  $X \otimes X$  measurements, referred to as biased fusion failures, give rise to a two-dimensional system symmetry [25] which considerably simplifies the decoding problem.

Our construction is motivated by dual-rail qubits in linear optics [26–29], the most widely studied platform for FBEC [3,19,23]. In this platform, fusions are inherently probabilistic and fail with a fixed probability. The failure probability can be exponentially suppressed using entangled ancillae with exponentially many photons [30], but it is difficult to suppress the failure probability below 25%. Notably, when a fusion fails, the  $X \otimes X$ information is erased but  $Z \otimes Z$  can be recovered [3,19]. Our construction leverages this bias to achieve a record threshold to fusion failures exceeding 25% in the experimentally relevant regime of nonzero loss rate per photon. This is the highest known threshold to fusion failures in linear optics without additional encodings on the resource states [3,24,31,32] and overcomes the 25% barrier, enabling scalable FBEC using an ancilla of only two entangled photons or four unentangled photons [30,33].

The XZZX cluster state.—We first review this instance of a generalized cluster state, a stabilizer state defined on a decorated graph G = (V, E) with two types of vertices  $V = \mathcal{X} \sqcup \mathcal{Z}$ . Each vertex represents a qubit; we refer to  $v \in \mathcal{X}$   $(v \in \mathcal{Z})$  as X-type (Z-type) qubits and denote them

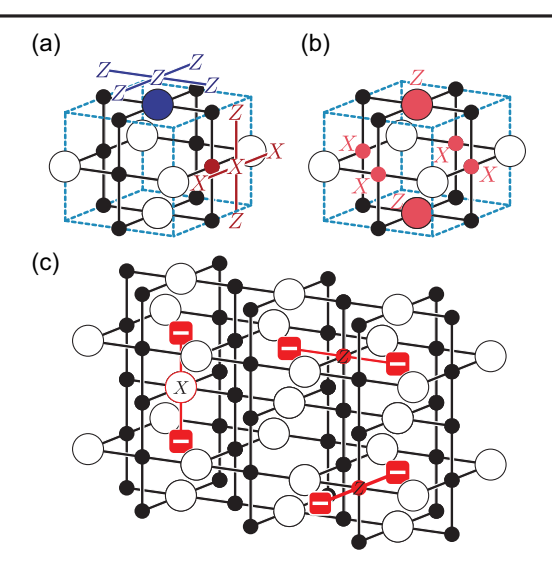


FIG. 1. (a) A unit cell of the XZZX cluster state, with two examples of face-centered stabilizers as in Eq. (1). (b) Multiplying the stabilizers centered at all faces of a unit cell produces the cell stabilizer. (c) X (Z) errors on Z-type (X-type) qubits causes neighboring cell stabilizers to flip to (-1). Z errors create defect pairs restricted to 2D planes, allowing for more effective decoding of biased noise.

by  $\bullet$  ( $\bigcirc$ ) [16]. The *N*-qubit generalized cluster state is the +1 eigenstate of *N* mutually commuting stabilizers, one centered at each qubit  $v \in V$ , given by

$$\begin{cases} X_{v} \prod_{(v,w) \in E} X_{w} \prod_{(v,u) \in E} Z_{u}, & v \in \mathcal{X} \\ w \in \mathcal{Z} & u \in \mathcal{X} \end{cases} \\ Z_{v} \prod_{\substack{(v,w) \in E \\ w \in \mathcal{Z}}} X_{w} \prod_{u \in \mathcal{X}} Z_{u}, & v \in \mathcal{Z} \end{cases}$$
(1)

The XZZX cluster state is defined on a periodic 3D graph, a unit cell of which is shown in Fig. 1(a) along with two face-centered stabilizers. The product of the face-centered stabilizers of a cell gives the cell stabilizer shown in Fig. 1(b), which is the product of the Z(X)-operator on Z-type (X-type) qubits on the faces of the unit cell.

A computation involves measuring all X-type (Z-type) qubits in the X (Z) basis. We can then reconstruct the values of the cell stabilizers to check for errors. An X (Z) error on a Z-type (X-type) qubit causes the qubit's two neighboring cell stabilizers to flip to (-1), as shown in Fig. 1(c). Z errors on X-type qubits only create defect pairs restricted to 2D planes. This 2D system symmetry simplifies the decoding problem—for example, a matching decoder only needs to match defects in 2D—and leads to higher thresholds for Z-biased noise [16,25].

We consider preparing this large entangled state by fusing copies of small entangled resource states, an approach standard to photonic dual-rail platforms [3,19,23,26,34]. We propose two schemes for the *XZZX* 

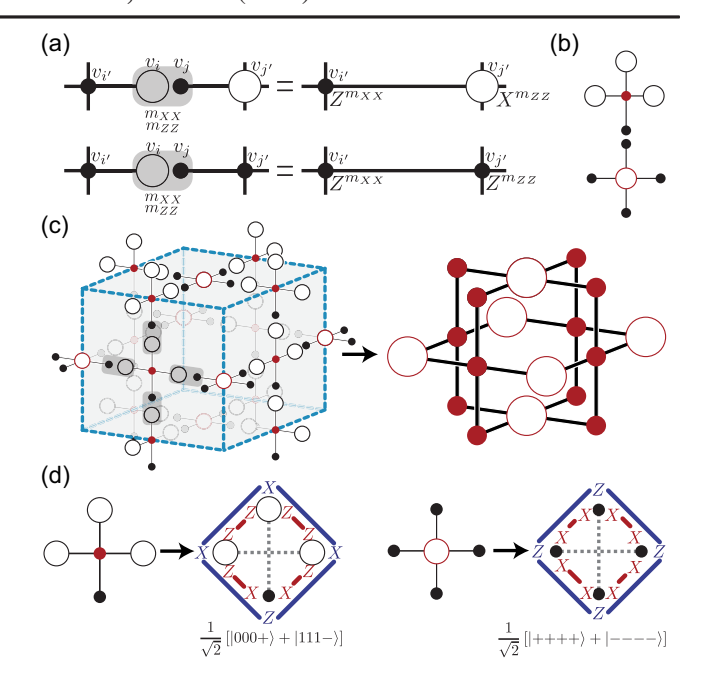


FIG. 2. The four-star construction. (a) Performing a fusion on a dangling pair of X- and Z-type qubits removes them from the cluster but forms an edge between their neighbors. (b) The two five-qubit cluster states we use in our construction. (c) The arrangement of five-qubit cluster states we use to build the XZZX cluster state. (d) We can equivalently start with four-qubit resource states resulting from measuring the center qubit as (0) in the X/Z basis.

cluster state, which are adaptations of schemes introduced in Ref. [3] for the RHG cluster state. The important distinction is that our resource states are modified to ensure that biased fusion failures create pairs of defects restricted to 2D planes, leading to improved thresholds.

Construction from four-star resource states.—We first introduce the principle underlying our construction. Let the cluster state defined on a graph G = (V, E) have a Z-type qubit at a degree-1 vertex  $v_i \in \mathcal{Z}$  with an edge to  $v_{i'}$ , and an X-type qubit at a degree-1 vertex  $v_i \in \mathcal{X}$  with an edge to  $v_{i'}$ with  $v_{i'} \neq v_{i'}$ . We refer to the qubits on degree-1 vertices as dangling qubits. As shown in Fig. 2(a), performing  $X_i \otimes X_j$  and  $Z_i \otimes Z_j$  measurements on the dangling qubits removes vertices  $v_i,\ v_j$  and edges  $(v_i,v_{i'}),\ (v_j,v_{j'})$ and adds a new edge  $(v_{i'}, v_{i'})$ . To ensure that the new cluster state is the +1 eigenstate of the new stabilizers created, a Pauli correction is applied to the qubits at  $v_{i'}$  and  $v_{i'}$  according to the outcomes of the  $X_i \otimes X_i$  and  $Z_i \otimes Z_i$ measurements  $(m_{XX}, m_{ZZ} = 0 \text{ or } 1)$ . If  $v_{i'} \in \mathcal{X}$  and  $v_{j'} \in \mathcal{Z} \ (v_{i'}, v_{j'} \in \mathcal{X}), \text{ the correction is } Z_{i'}^{m_{XX}} \otimes X_{j'}^{m_{ZZ}}$  $(Z_{i'}^{m_{XX}} \otimes Z_{i'}^{m_{ZZ}})$ . Observe that for unreliable  $X_i \otimes X_j$  measurements, we cannot correctly determine the proper Pauli correction on  $v_{i'}$ , which is equivalent to applying I or Z to the X-type qubit at  $v_{i'}$  with 50% probability (see Supplemental Material [35] for details).

We now introduce the two five-qubit cluster states shown in Fig. 2(b) with stabilizers defined according to Eq. (1). One has a Z-type qubit at the center and the other has an X-type qubit. The center qubits marked in red will eventually form the XZZX cluster state. The Z-centered (X-centered) states are placed at the location of Z-type (X-type) qubits, as shown in Fig. 2(c), such that neighboring dangling qubits are always opposite types and can be fused according to Fig. 2(a). Finally, the cluster state qubits can be measured in the appropriate basis.

Note that each center qubit is entangled into the final cluster state after four fusions on its neighboring dangling qubits; consequently, four Pauli corrections need to be accounted for on this qubit. This may be done in software by simply reinterpreting the outcome of its final measurement. This is because an X(Z) measurement of an X-type (Z-type) qubit after a Pauli Z(X) correction is equivalent to an X(Z) measurement followed by a classical flip of the measurement outcome  $0 \leftrightarrow 1$ .

We can simplify the five-qubit resource states to fourqubit resource states because measuring cluster state qubits commutes with fusions. That is, we can measure the resource states' center qubits *before* the fusion measurements, and account for Pauli corrections in software. Measuring the center X-type (Z-type) qubits of the fivequbit states in the X (Z) basis with outcome 0 produces the four-star resource states in Fig. 2(d). Indeed, we can directly start with the four-star resource states, in which case the central qubit becomes a virtual qubit that is never physically realized or measured, whose effective measurement outcome is entirely tracked in software [3].

Construction from six-ring resource states.—Our second construction is based on fusing two qubits of the same type. While our construction is reminiscent of the approach in [3], we provide an alternate derivation.

Consider a cluster state defined on a graph G = (V, E)with two Z-type (X-type) qubits at vertices  $v_i, v_j \in V$  such that  $v_i$  and  $v_j$  are not neighbors and share no neighbors. Measuring  $X_i \otimes X_j$   $(Z_i \otimes Z_j)$  on these qubits projects them into an effective two-dimensional subspace with Pauli operators  $\bar{X} = X_i \ (X_i \otimes X_i)$  and  $\bar{Z} = Z_i \otimes Z_i \ (Z_i)$ . As shown in Fig. 3(a), a new cluster state is obtained with vertices  $v_i$ ,  $v_j$  replaced by a single vertex  $v_{ij}$  with an effective Z-type (X-type) qubit. All vertices originally connected to either  $v_i$  or  $v_j$  are connected to  $v_{ij}$  in the new graph. To ensure that the new cluster state is the +1eigenstate of all the stabilizers, a Pauli correction determined by the  $X_i \otimes X_i$   $(Z_i \otimes Z_i)$  measurement outcome,  $m_{XX}(m_{ZZ}) = 0$  or 1, must be applied to the qubits originally adjacent to  $v_i$ . Specifically,  $Z^{m_{XX}}$   $(Z^{m_{ZZ}})$  is applied to adjacent X-type qubits and  $X^{m_{XX}}$  ( $X^{m_{ZZ}}$ ) is applied to adjacent Z-type qubits.

We introduce the six-ring resource state in Fig. 3(b). A copy of this state is placed at two opposite corners of each unit cell as in Fig. 3(c). Two qubits of the same type share a

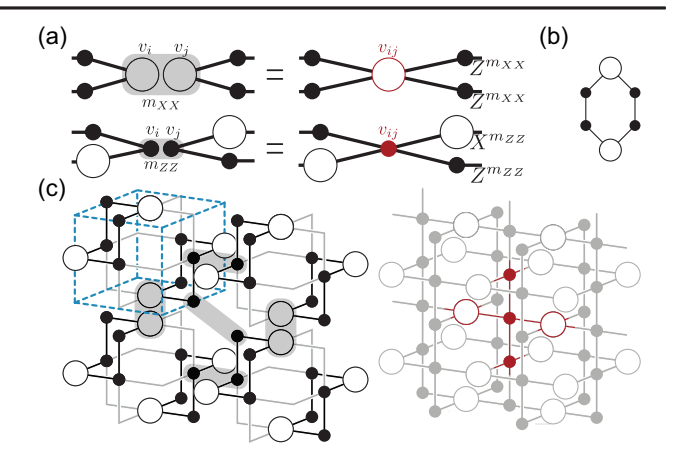


FIG. 3. The six-ring construction. (a) Measuring  $X_i \otimes X_j$   $(Z_i \otimes Z_j)$  on two Z-type (X-type) qubits projects those qubits onto a two-dimensional subspace with effective Pauli operators  $\bar{X}_{ij} = X_i$ ;  $(X_i \otimes X_j)$  and  $\bar{Z}_{ij} = Z_i \otimes Z_j$   $(Z_i)$ , with all edges to neighbors intact. (b) The six-ring resource state. (c) The fusion pattern used to join the six-ring states to make the XZZX cluster state.

face or edge center. If we measure  $X \otimes X$  ( $Z \otimes Z$ ) for each pair of Z-type (X-type) qubits sharing a face or edge, and apply the Pauli corrections, we obtain the XZZX cluster state comprised of the effective qubits. Note that an unreliable  $X \otimes X$  measurement on Z-type qubits leads to an incorrect Pauli Z correction to adjacent X-type qubits. Finally, we measure the effective Pauli  $\bar{Z} = Z \otimes Z$  of the effective Z-type qubits, and the effective Pauli  $\bar{X} = X \otimes X$ of the effective X-type qubits. Note that an unreliable  $\bar{X} =$  $X \otimes X$  measurement on an effective X-type qubit is like a  $\bar{Z}$ error on that qubit. As before, Pauli corrections from the first set of measurements that create the cluster state can be tracked in software by reinterpreting the outcomes of the second set of measurements. The above discussion implies that biased fusion failures lead to heralded Z errors on X-type qubits in the XZZX cluster state.

Application to dual-rail qubits with linear-optic fusions.—A photonic dual-rail qubit is given by a single photon in one of two orthogonal modes,  $|\bar{0}\rangle = |01\rangle$ ,  $|\bar{1}\rangle = |10\rangle$ , and is a leading candidate for linear-optical quantum computing [19,26,29,40]. All single qubit gates can be performed deterministically using passive linear optical elements [41]. Multiqubit operations, like fusions, are nondeterministic. Here, fault-tolerant FBEC is based on heralded generation of few-body entangled resource states, followed by nondeterministic fusion measurements [3,23]. Remarkably, the resource states we introduce differ from the ones considered in previous works [3] only by Hadamard transformations, and these states can be easily generated using linear-optics circuits [35]. Fusion measurements can be realized using a "type-II" fusion circuit comprised of beam splitters and photon number resolving detectors [19,28]. The circuit consumes the two qubits being fused and outputs the photon number clicks observed at each detector. Depending on the observed clicks, one of two measurements are performed: (1) successful  $X \otimes X$ and  $Z \otimes Z$  measurements, in which case we say the fusion succeeded, or (2) independent single-qubit Z measurements, in which case we say that the fusion failed. In both cases, measurement outcomes are inferred from detector clicks [3,35]. In a failed fusion,  $Z \otimes Z$  can be recovered by multiplying the independent Z measurement outcomes, while the  $X \otimes X$  measurement is completely erased. Without any ancilla photons, the probability of fusion failure is  $p_{\text{fail}} = 1/2$  [19]. With a  $(2^n - 2)$ -photon entangled ancilla, for a total of  $2^n$  photons in the fusion circuit, the failure probability may be reduced to  $p_{\text{fail}} =$  $1/2^n$  [30]. For the particular case of n=2, the failure probability may also be reduced to 1/4 with a fourphoton unentangled ancilla [33]. However, n > 2 requires entangled states that get progressively more complicated to

Beyond fusion failures, our system may also suffer from photon loss. A loss of any photon in the fusion circuit is heralded by observing fewer than expected clicks at the detector and results in an erasure of both  $X \otimes X$  and  $Z \otimes Z$  measurement outcomes. If the probability of loss per photon is  $p_{\text{loss}}$ , then the probability of an erasure in the boosted fusion circuit with a total of  $1/p_{\text{fail}}$  photons is  $p_{\text{full erase}} = 1 - (1 - p_{\text{loss}})^{1/p_{\text{fail}}}$  [3]. Evidently, there is a tradeoff between the rate at which  $X \otimes X$  outcomes are erased due to fusion failure and the rate at which both outcomes are erased due to photon loss.

We evaluate our fusion architectures' performance under the linear optical error model. The solid red (blue) curve in Fig. 4 gives the thresholds for the four-star (six-ring) construction. If  $(p_{\rm fail}, p_{\rm loss})$  lies under a curve, then these errors are correctable, otherwise not. We also compare our results with the thresholds obtained with (a) the four-star

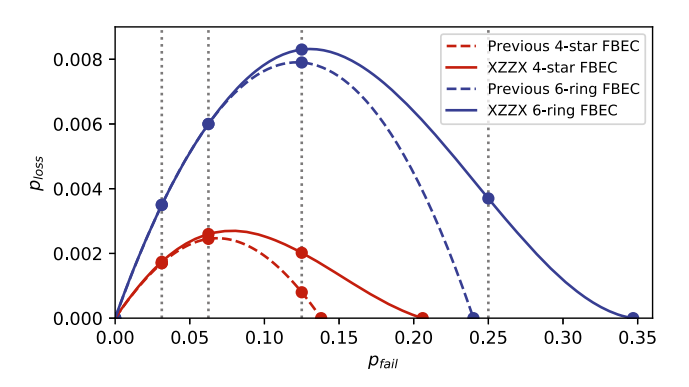


FIG. 4. Numerically simulated thresholds with our four-star (red) and six-ring (blue) construction protocols under the linear optical error model. For comparison, thresholds based on previous approaches which do not leverage the noise bias in fusion failures are also shown [3,32]. From left to right, dotted vertical lines represent fusions boosted by 30, 14, 6, and 2 entangled ancilla photons.

and six-ring construction from a previous work [3] to construct the *XZZX* cluster state and (b) our four-star and six-ring constructions based on the adaptive error-correction strategy introduced in [32]. The thresholds with both (a) and (b), shown in Fig. 4 using dashed lines, are identical and consistent with known results [3].

Thresholds for the six-ring construction are higher than the four-star construction as it has fewer fusions per unit cell, and hence a lower probability of error. When  $p_{\rm loss}=0$ , the numerically obtained threshold for biased fusion failure using our scheme is 34.7% (20.6%) for the six-ring (four-star) construction. These thresholds can also be derived analytically (see [35]) and are significantly higher than the threshold obtained with previous proposals that fail to leverage the bias in fusion failures, correspondingly  $\sim 24\%$  ( $\sim 14.5\%$ ) [3]. This is because in our approach fusion failure leads to a 2D syndrome graph which is easier to decode than the three-dimensional graphs of previous strategies.

When  $p_{\rm loss} \neq 0$ , we must deal with full fusion erasure along with fusion failure. For a fixed  $p_{\rm loss}$ , decreasing  $p_{\rm fail}$  by adding more photons increases the probability of  $p_{\rm full~erase}$ . This tradeoff gives the overall "inverted-u" shape of the threshold curve. Importantly, we see that our six-ring construction can tolerate up to  $p_{\rm loss} \leq 0.37\%$  when  $p_{\rm fail} = 25\%$ . Hence, it is possible to achieve fault tolerance with only two entangled ancilla photons for boosted fusions [30], or alternatively with four unentangled ancilla photons for boosted fusions [33] when  $p_{\rm loss} \leq 0.25\%$ . In contrast, the previous six-ring scheme could only tolerate  $p_{\rm fail} \lesssim 24\%$ , making it impossible to achieve fault tolerance with these simple ancillae.

Conclusion.—By taking advantage of the biased structure of fusion failures, we introduce new resource states and fusion strategies for FBEC that allow for their more efficient error correction. This FBEC strategy is particularly relevant to linear-optical quantum computers using dual-rail qubits, where biased fusion failures are the dominant source of error. Our resource states and fusion strategies require no additional overhead to realize compared to the previous approach of Ref. [3], but result in higher thresholds to fusion failures for both four-star and six-ring constructions. In particular, our six-ring construction has a threshold to fusion failures over 25%, which can be reached using only a two-photon entangled ancilla or a four-photon unentangled ancilla, overcoming a key barrier for photonic quantum computing.

Our construction achieves higher thresholds because linear optical fusions naturally introduce *Z* errors, we construct our cluster state so that *Z* errors do not propagate to *X* or *Y* errors, and the *XZZX* cluster state is tailored to correct *Z* errors [16]. Our construction can likely also be used to improve thresholds to fusion failures in other fusion-based schemes, such as the encoded resource states in [3] and the 1D resource states in [24], by modifying the

fusion measurements to ensure lower dimensional decoding graphs. A similar strategy should apply to any hardware with biased entangling errors. The *XZZX* cluster state construction used in this work has already led to the development of a high-threshold fusion-based architecture with atoms [42]. Investigating additional hardware that can benefit from our approach is left to future work.

We are grateful to James D. Teoh, Harshvardhan K. Babla and Yue Wu for helpful discussions. We thank the Yale Center for Research Computing for use of the Grace cluster. This material is based on work supported by the National Science Foundation (NSF) under Grant No. 2137740. Any opinions, findings, and conclusions or recommendations expressed in this publication are those of the authors and do not necessarily reflect the views of NSF.

Note added.—Recently, Ref. [43] appeared reinterpreting our construction as a choice of the fusion failure basis for creating the RHG cluster state. This work also introduces further strategies to dynamically choose fusion failure bases and levels of boosting to improve error tolerance beyond reducing the dimensionality of the decoding graph.

- [1] N. C. Menicucci, P. van Loock, M. Gu, C. Weedbrook, T. C. Ralph, and M. A. Nielsen, Phys. Rev. Lett. 97, 110501 (2006).
- [2] J. E. Bourassa, R. N. Alexander, M. Vasmer, A. Patil, I. Tzitrin, T. Matsuura, D. Su, B. Q. Baragiola, S. Guha, G. Dauphinais *et al.*, Quantum 5, 392 (2021).
- [3] S. Bartolucci, P. Birchall, H. Bombin, H. Cable, C. Dawson, M. Gimeno-Segovia, E. Johnston, K. Kieling, N. Nickerson, M. Pant *et al.*, Nat. Commun. 14, 912 (2023).
- [4] H. J. Briegel and R. Raussendorf, Phys. Rev. Lett. 86, 910 (2001).
- [5] R. Raussendorf and H. J. Briegel, Phys. Rev. Lett. 86, 5188 (2001).
- [6] R. Raussendorf, D. Browne, and H. Briegel, J. Mod. Opt. 49, 1299 (2002).
- [7] R. Raussendorf, D. E. Browne, and H. J. Briegel, Phys. Rev. A 68, 022312 (2003).
- [8] H. J. Briegel, D. E. Browne, W. Dür, R. Raussendorf, and M. Van den Nest, Nat. Phys. 5, 19 (2009).
- [9] R. Raussendorf, J. Harrington, and K. Goyal, Ann. Phys. (Amsterdam) **321**, 2242 (2006).
- [10] R. Raussendorf and J. Harrington, Phys. Rev. Lett. 98, 190504 (2007).
- [11] A. Bolt, G. Duclos-Cianci, D. Poulin, and T. M. Stace, Phys. Rev. Lett. 117, 070501 (2016).
- [12] B. J. Brown and S. Roberts, Phys. Rev. Res. 2, 033305 (2020).
- [13] R. Raussendorf, J. Harrington, and K. Goyal, New J. Phys. **9**, 199 (2007).
- [14] R. Raussendorf, S. Bravyi, and J. Harrington, Phys. Rev. A 71, 062313 (2005).

- [15] A. Y. Kitaev, in *Quantum Communication, Computing, and Measurement* (Springer, New York, 1997), pp. 181–188.
- [16] J. Claes, J. E. Bourassa, and S. Puri, npj Quantum Inf. 9, 9 (2023).
- [17] X.-G. Wen, Phys. Rev. Lett. 90, 016803 (2003).
- [18] J. P. Bonilla Ataides, D. K. Tuckett, S. D. Bartlett, S. T. Flammia, and B. J. Brown, Nat. Commun. 12, 1 (2021).
- [19] D. E. Browne and T. Rudolph, Phys. Rev. Lett. 95, 010501 (2005).
- [20] K. Fukui, A. Tomita, A. Okamoto, and K. Fujii, Phys. Rev. X 8, 021054 (2018).
- [21] K. Fukui, Phys. Rev. A 107, 052414 (2023).
- [22] R. Chao, M. E. Beverland, N. Delfosse, and J. Haah, Quantum 4, 352 (2020).
- [23] Y. Li, P. C. Humphreys, G. J. Mendoza, and S. C. Benjamin, Phys. Rev. X 5, 041007 (2015).
- [24] S. Paesani and B. J. Brown, Phys. Rev. Lett. 131, 120603 (2023).
- [25] B. J. Brown, arXiv:2207.06428.
- [26] M. A. Nielsen, Phys. Rev. Lett. 93, 040503 (2004).
- [27] M. A. Nielsen and C. M. Dawson, Phys. Rev. A **71**, 042323 (2005).
- [28] A. Gilchrist, A. J. F. Hayes, and T. C. Ralph, Phys. Rev. A 75, 052328 (2007).
- [29] P. Kok, W. J. Munro, K. Nemoto, T. C. Ralph, J. P. Dowling, and G. J. Milburn, Rev. Mod. Phys. 79, 135 (2007).
- [30] W. P. Grice, Phys. Rev. A 84, 042331 (2011).
- [31] Y. Li, S. D. Barrett, T. M. Stace, and S. C. Benjamin, Phys. Rev. Lett. **105**, 250502 (2010).
- [32] J. M. Auger, H. Anwar, M. Gimeno-Segovia, T. M. Stace, and D. E. Browne, Phys. Rev. A 97, 030301(R) (2018).
- [33] F. Ewert and P. van Loock, Phys. Rev. Lett. **113**, 140403 (2014).
- [34] D. A. Herrera-Martí, A. G. Fowler, D. Jennings, and T. Rudolph, Phys. Rev. A 82, 032332 (2010).
- [35] See Supplemental Material at http://link.aps.org/supplemental/10.1103/PhysRevLett.131.120604, which includes Refs. [36–39] for more details on the four-star and six-ring constructions, boosted type-II fusions, and an analytic derivation of the thresholds against pure biased fusion failure.
- [36] M. Varnava, D. E. Browne, and T. Rudolph, Phys. Rev. Lett. 100, 060502 (2008).
- [37] N. Delfosse and G. Zémor, Phys. Rev. Res. **2**, 033042 (2020).
- [38] T. M. Stace, S. D. Barrett, and A. C. Doherty, Phys. Rev. Lett. **102**, 200501 (2009).
- [39] M. F. Sykes and J. W. Essam, J. Math. Phys. (N.Y.) 5, 1117 (1964).
- [40] E. Knill, R. Laflamme, and G. J. Milburn, Nature (London) **409**, 46 (2001).
- [41] A. Politi, J. C. Matthews, M. G. Thompson, and J. L. O'Brien, IEEE J. Sel. Top. Quantum Electron. **15**, 1673 (2009).
- [42] K. Sahay, J. Jin, J. Claes, J. D. Thompson, and S. Puri, arXiv:2302.03063.
- [43] H. Bombín, C. Dawson, N. Nickerson, M. Pant, and J. Sullivan, arXiv:2303.16122.